A&A 595, A57 (2016)
DOI: 10.1051/0004-6361/201628809

Astronomy & Astrophysics

Polarization measurement analysis

III. Analysis of the polarization angle dispersion function with high precision polarization data

D. Alina[1,3], L. Montier[2,3], I. Ristorcelli[2,3], J.-P. Bernard[2,3], F. Levrier[4], and E. Abdikamalov[1]

[1] Department of Physics, School of Science and Technology, Nazarbayev University, 010000 Astana, Kazakhstan
e-mail: dana.alina@nu.edu.kz
[2] Université de Toulouse, UPS-OMP, IRAP, 31028 Toulouse Cedex 4, France
[3] CNRS, IRAP, 9 Av. colonel Roche, BP 44346, 31028 Toulouse Cedex 4, France
[4] LERMA/LRA – ENS Paris et Observatoire de Paris, 24 rue Lhomond, 75231 Paris Cedex 05, France

Received 28 April 2016 / Accepted 4 August 2016

ABSTRACT

High precision polarization measurements, such as those from the *Planck* satellite, open new opportunities for the study of the magnetic field structure as traced by polarimetric measurements of the interstellar dust emission. The polarization parameters suffer from bias in the presence of measurement noise. It is critical to take into account all the information available in the data in order to accurately derive these parameters. In our previous work, we studied the bias on polarization fraction and angle, various estimators of these quantities, and their associated uncertainties. The goal of this paper is to characterize the bias on the polarization angle dispersion function that is used to study the spatial coherence of the polarization angle. We characterize for the first time the bias on the conventional estimator of the polarization angle dispersion function and show that it can be positive or negative depending on the true value. Monte Carlo simulations were performed to explore the impact of the noise properties of the polarization data, as well as the impact of the distribution of the true polarization angles on the bias. We show that in the case where the ellipticity of the noise in (Q, U) varies by less than 10%, one can use simplified, diagonal approximation of the noise covariance matrix. In other cases, the shape of the noise covariance matrix should be taken into account in the estimation of the polarization angle dispersion function. We also study new estimators such as the dichotomic and the polynomial estimators. Though the dichotomic estimator cannot be directly used to estimate the polarization angle dispersion function, we show that, on the one hand, it can serve as an indicator of the accuracy of the conventional estimator and, on the other hand, it can be used for deriving the polynomial estimator. We propose a method for determining the upper limit of the bias on the conventional estimator of the polarization angle dispersion function. The method is applicable to any linear polarization data set for which the noise covariance matrices are known.

Key words. polarization – methods: statistical – methods: data analysis – techniques: polarimetric

1. Introduction

The linear polarization of the incoming radiation can be described by the Stokes parameters Q and U along with the total intensity I. The polarization fraction p and the polarization angle ψ are derived from I, Q and U, and bias on these parameters appears in the presence of measurement noise (Serkowski 1958; Wardle & Kronberg 1974; Simmons & Stewart 1985; Vaillancourt 2006; Quinn 2012). This issue has recently been addressed by Montier et al. (2015a,b), hereafter Papers I and II of this series on the polarization measurement analysis of high precision data. In this work, which we refer to as Paper III, we aim to characterize the bias on the polarization angle dispersion function – a polarization parameter that measures the spatial coherence of the polarization angle.

The interstellar magnetic field structure can be revealed by the polarimetric measurements of synchrotron radiation and of dust thermal emission and extinction (Mathewson & Ford 1970; Han 2002; Beck & Gaensler 2004; Heiles & Troland 2005; Fletcher 2010). The interstellar dust particles are aligned with respect to the magnetic field (Hall & Mikesell 1949; Hiltner 1949; Lazarian & Hoang 2008). This leads to linear polarization in the visible, infrared and submillimetre (Benoît et al. 2004; Vaillancourt 2007; Andersson et al. 2015). The interstellar dust polarization yields information about the direction of the plane of the sky (POS) component of the magnetic field. Heiles (1996) have used observations of polarization by dust extinction and found that the inclination of the Galactic magnetic field with respect to the plane of the disk of matter is about 7°. Recently Planck Collaboration Int. XIX (2015) have derived the all-sky magnetic field direction map as projected onto the POS from the *Planck* Satellite data. They have also used the polarization angle dispersion function and have studied its correlation with the polarization fraction. In the framework of their analysis, the observed anti-correlation allows to come to a conclusion that the observed polarization at large scales (diffuse ISM, large molecular clouds) largely depends on the magnetic field structure. Polarimetric measurement of the emission from molecular clouds and star forming regions help to better understand the role of the magnetic field in star formation (Matthews et al. 2009; Dotson et al. 2010; Tang et al. 2012; Zhang et al. 2010; Cortes et al. 2016).

Davis & Greenstein (1951) and Chandrasekhar & Fermi (1953) have calculated the angular dispersion in polarimetric

measurements of distant stars (Hiltner 1951) to derive the strength of the magnetic field in the local spiral arm. Since then, the so-called Davis-Chandrasekhar-Fermi method has been widely used to derive some properties of the magnetic field such as the strength of its POS component (Lai et al. 2001; Sandstrom et al. 2002; Crutcher et al. 2004; Girart et al. 2006; Falceta-Gonçalves et al. 2008). In fact, this method is based on the polarization angle structure function, which is obtained as the average of the polarization angle dispersion function over the positions. The polarization angle structure function is also used to study the magnetic field direction that can be inferred from different types of polarimetric measurements. For example, Mao et al. (2010) computes the polarization angle structure function in order to study the structures traced by the synchrotron Faraday rotation measures.

Serkowski (1958) have shown that the structure function of the Stokes parameters Q and U reaches a limit. When the area, considered to calculate the structure function, becomes too large and includes non-connected regions, the parameters become spatially decorrelated. Poidevin et al. (2010) reports a similar behavior of the polarization angle structure function. The randomness of angles can be due not only to the physical decorrelation in the underlying pattern, but also to the noise of the measurement. According to Hildebrand et al. (2009), the polarization angle structure function contains contributions of the large-scale and turbulent magnetic field components. They have developed a method to estimate the strength of these components using the polarization angle structure function. The method has successfully been applied to polarimetry and interferometry data to characterize the magnetic turbulence power spectrum and magnetic field strength in molecular clouds (Houde et al. 2011a,b, 2016). The authors claim that its uncertainty can simply be calculated through the uncertainties of the angles used in the determination of the polarization angle structure function.

We have shown in Papers I and II that in order to accurately estimate the polarization fraction and polarization angle, one should take into account the full noise covariance matrix if possible. In this work, we study the behavior of the bias on the polarization angle dispersion function knowing the full noise covariance matrix and the distribution of the true polarization angles. We introduce new estimators of the polarization angle dispersion function and describe a method to evaluate an upper limit for the bias of the conventional estimator.

In Sect. 2 we introduce the notations and give the definition of the conventional estimator of the polarization angle dispersion function in terms of the Stokes parameters. In Sect. 3 we demonstrate the peculiarity of the bias. We also discuss the impact on the bias of the noise covariance matrix and of the distribution of the true polarization angles in the vicinity of the point of interest. We address the reliability of the conventional uncertainty on polarization angle dispersion function as well. In Sect. 4 we introduce alternative estimators and propose a method to evaluate the maximum bias of the conventional estimator for a given set of data.

2. Conventional estimator of the polarization angle dispersion function

2.1. Definition and notations

A POS component of polarized radiation is characterized by the true, that is, not affected by the measurement noise, polarization fraction

$$p_0 = \frac{\sqrt{Q_0^2 + U_0^2}}{I_0}, \tag{1}$$

and polarization orientation angle

$$\psi_0 = \frac{1}{2}\arctan(U_0,\, Q_0), \tag{2}$$

where I_0, Q_0, U_0 are the true Stokes parameters that describe the intensity and the linear polarization of the incoming radiation. Function arctan takes two arguments in order to choose the correct quadrant when calculating the arctangent of the ratio U/Q.

The true polarization angle dispersion function at the position $\boldsymbol{x}$, where $\boldsymbol{x}$ is the 2D coordinate in the POS, is defined as the root mean square over the $N(l)$ pairs of angles located within an area of radius l around $\boldsymbol{x}$ (see Fig. 1 for illustration):

$$\mathcal{S}_0(\boldsymbol{x}, l) = \sqrt{\frac{1}{N(l)}\sum_{i=1}^{N(l)}[\psi_0(\boldsymbol{x}) - \psi_0(\boldsymbol{x}+\boldsymbol{l}_i)]^2}. \tag{3}$$

$\mathcal{S}_0$ takes values between 0 and $\pi/2$. We note that it is also possible to consider only the angles contained in an annulus of a certain radius and width. In that case $\mathcal{S} = \mathcal{S}(\boldsymbol{x}, l, \delta)$, where δ is the width of the annulus and l is the lag.

When using the measured quantities, we will call this estimator the "conventional estimator" and denote it by $\hat{\mathcal{S}}_{\rm C}$:

$$\hat{\mathcal{S}}_{\rm C}(\boldsymbol{x}, l) = \sqrt{\frac{1}{N(l)}\sum_{i=1}^{N(l)}[\psi(\boldsymbol{x}) - \psi(\boldsymbol{x}+\boldsymbol{l}_i)]^2}. \tag{4}$$

The above formula takes the following form in terms of the Stokes Q and U parameters:

$$\mathcal{S}(\boldsymbol{x}, l) = \left[\frac{1}{N(l)}\sum_{i=1}^{N(l)}\left(\frac{1}{2}\arctan[U(\boldsymbol{x})Q(\boldsymbol{x}+\boldsymbol{l}_i) - Q(\boldsymbol{x})U(\boldsymbol{x}+\boldsymbol{l}_i),\right.\right.$$
$$\left.\left.Q(\boldsymbol{x})Q(\boldsymbol{x}+\boldsymbol{l}_i) + U(\boldsymbol{x})U(\boldsymbol{x}+\boldsymbol{l}_i)]\right)^2\right]^{1/2}. \tag{5}$$

This equation is applicable to both $\hat{\mathcal{S}}_{\rm C}$ and $\mathcal{S}_0$.

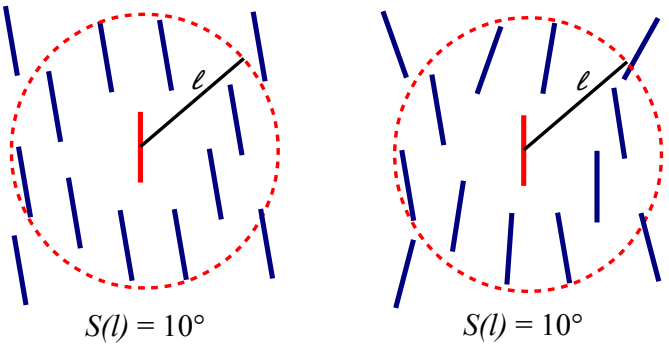

Fig. 1. Schematic view of the simulated configuration of polarization orientations. The polarization angle dispersion function is calculated at the position of the red line segment within the red-dotted circle of radius l. *Left*: uniform configuration. *Right*: random configuration. Both cases give $\mathcal{S} = 10°$.

Noise on any polarimetric measurement is characterized by a noise covariance matrix Σ. The noise covariance matrix of a linear polarization measurement has the following form:

$$\Sigma \equiv \begin{pmatrix} \sigma_I^2 & \sigma_{IQ} & \sigma_{IU} \\ \sigma_{IQ} & \sigma_Q^2 & \sigma_{QU} \\ \sigma_{IU} & \sigma_{QU} & \sigma_U^2 \end{pmatrix}, \tag{6}$$

where σ_X^2 ($X = I, Q, U$) characterizes the noise level in the X parameter (i.e., variance), and σ_{XY} ($Y = I, Q, U$) characterizes the correlation between noise on X and Y (i.e., covariance).

As we are interested only in the angle measurements, the intensity is assumed to be known exactly, so that the noise covariance matrix can be reduced to:

$$\Sigma_p = \begin{pmatrix} \sigma_Q^2 & \sigma_{QU} \\ \sigma_{QU} & \sigma_U^2 \end{pmatrix}. \tag{7}$$

It is possible to fully characterize Σ_p using only two parameters (Montier et al. 2015a):

$$\varepsilon_{\rm eff}^2 = \frac{1 + \varepsilon^2 + \sqrt{(\varepsilon^2 - 1)^2 + 4\rho^2\varepsilon^2}}{1 + \varepsilon^2 - \sqrt{(\varepsilon^2 - 1)^2 + 4\rho^2\varepsilon^2}} \tag{8}$$

and

$$\theta = \frac{1}{2}\arctan\left(\frac{2\rho\varepsilon}{\varepsilon^2 - 1}\right). \tag{9}$$

Here ε and ρ are the ellipticity and correlation between noises on Q and U:

$$\rho = \frac{\sigma_{QU}}{\sigma_Q \sigma_U} \quad \text{and} \quad \varepsilon = \frac{\sigma_U}{\sigma_Q}. \tag{10}$$

The reduced noise covariance matrix then takes the following form:

$$\Sigma_p = \frac{\sigma_p^2}{\sqrt{1-\rho^2}} \begin{pmatrix} 1/\varepsilon & \rho \\ \rho & \varepsilon \end{pmatrix}, \tag{11}$$

where σ_p is a global polarization noise scaling factor, such that $\det(\Sigma_p) = \sigma_p^4$ (Montier et al. 2015a).

The effective ellipticity $\varepsilon_{\rm eff}$ and the angle θ give the shape of the noise distribution in linear polarization, independently of the reference frame to which Q and U are attached.

In order to characterize the form of the noise covariance matrix, 3 regimes of $\varepsilon_{\rm eff}$ are considered in this study:

- the *canonical* case: $\varepsilon_{\rm eff} = 1$. This corresponds to the equality and independence between noise levels on Q and U: $\sigma_Q^2 = \sigma_U^2$, $\sigma_{UQ} = \sigma_{UQ} = 0$;
- the *low* regime: $1 \leq \varepsilon_{\rm eff} < 1.1$. This means that the differences and/or correlations between noise levels on Q and U are small;
- the *extreme* regime: $1.1 \leq \varepsilon_{\rm eff} < 2$. This means that the differences and/or correlations between noise levels on Q and U are large.

2.2. Monte Carlo simulations

In order to characterize the bias on the polarization angle dispersion function, we perform Monte Carlo (MC) simulations. We build numerical distribution functions (DFs) of $\hat{\mathcal{S}}_{\rm C}$ using the following set of basic assumptions:

1. We consider 10 pixels: 1 central pixel and 9 adjacent pixels to be contained within a circle of radius l, as shown in Fig. 1. In a regularly-gridded map there are 8 adjacent pixels, but a small difference (by 1 or 2) in the number of pixels does not affect the results of our simulations.
2. All pixels have the same true polarization fraction $p_0 = 0.1$ and the same noise covariance matrix Σ_p. The latter assumption seems to be reasonable because $\mathcal{S}$ is usually calculated inside small areas, where the instrumental noise does not change much.
3. We perform $N_{\rm MC} = 10^6$ noise realizations at each run (i.e., for each simulated configuration, including the signal-to-noise ratio (S/N), the true value, the shape of the noise covariance matrix and the true polarization angles).
4. We consider Gaussian noise on Q and U with a noise covariance matrix Σ_p.
5. We vary the S/N of p between 0.1 and 30. We set $\sigma_p = p_0/(S/N)$ to be used in Eq. (11).
6. We vary ρ in the range $[-0.5, 0.5]$ and ϵ in the range $[0.5, 2]$. The low regime is obtained when using $\rho \simeq 0$ and $\varepsilon \simeq 1$; other cases (with $\epsilon \leq 0.9$, and $\epsilon \geq 1.1$ and $\rho \geq |0.05|$) give the *extreme* regime of $\varepsilon_{\rm eff}$.

We use $\psi_{0,i}$ to denote the true polarization angle for pixel i, and consider two cases of the configuration: the "uniform" and the "random" configurations. In the uniform configuration, all angles $\psi_{0,i}$ are the same for $i \in [1, 9]$, while $\psi_{0,0}$ is calculated as:

$$\psi_{0,0} = \psi_{0,i} - \mathcal{S}_0. \tag{12}$$

In the random configuration $\psi_{0,i}$ for $i \in [1, 9]$ are generated randomly and $\psi_{0,0}$ is selected from a series of random values to obtain $\mathcal{S}_0$ with $(10^{-5})^\circ$ precision using Equation 3 at each run. Examples of both configurations, uniform and random, are illustrated on left and right panels in Fig. 1, respectively. There are 10 representative sets of the true angles for each configuration and the true polarization angle dispersion function. They are obtained by varying $\psi_{0,0}$ from 0 to $\pi/2$ with 10° ($\pi/18$) step for the uniform configuration and by generating additional sets for the random configuration.

Once $\psi_{0,0}$ and $\psi_{0,i}$ are obtained, the following transformation is performed in order to get the corresponding Q and U parameters:

$$Q_{0,i} = p_0 I_0 \cos(2\psi_{0,i}),\ i \in [0, 9], \tag{13}$$

$$U_{0,i} = p_0 I_0 \sin(2\psi_{0,i}),\ i \in [0, 9], \tag{14}$$

with $I_0 = 1$. Random Gaussian noise is generated for each pixel for Q and U according to the noise covariance matrix and is added to the true values to obtain the simulated Stokes parameters for each pixel. The simulated measured polarization angle dispersion function $\hat{\mathcal{S}}_{\rm C}$ is calculated using Eq. (5).

Once we have the simulated sample of 10^6 values of $\hat{\mathcal{S}}_{\rm C}$ for the given $\mathcal{S}_0$, the configuration of the true angles and the noise level, we can build numerical DFs, which we denote as $f(\hat{\mathcal{S}}_{\rm C} \,|\, \mathcal{S}_0, \Sigma)$. The shape of the DF for the given noise levels in the *canonical* case of the noise covariance matrix and in the uniform configuration of the true angles is illustrated in Fig. 2. At very low S/Ns, the distribution function peaks at $\pi/\sqrt{12}$, regardless of $\mathcal{S}_0$. The value $\pi/\sqrt{12}$ ($\simeq$51.96°) corresponds to the result of $\mathcal{S}$ with purely random distribution of angles. In fact, for a pair

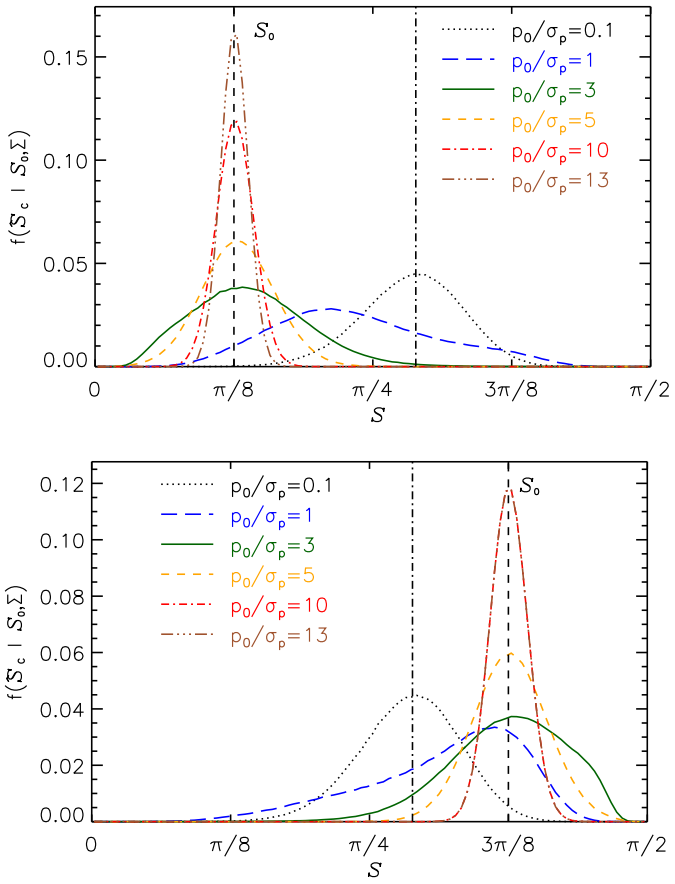

Fig. 2. Examples of the simulated distribution functions of the conventional estimator of the dispersion function $\hat{\mathcal{S}}_C$ for different S/Ns of p in the *canonical* case of the noise covariance matrix. *Top*: $\mathcal{S}_0 = \pi/8$, *bottom*: $\mathcal{S}_0 = 3\pi/8$. The vertical dashed line shows the true value, and the vertical dash-dotted line shows the value of $\pi/\sqrt{12}$.

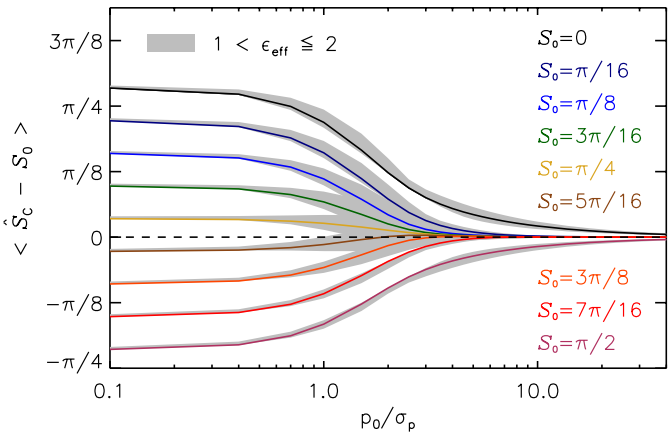

Fig. 3. Average bias on 10^6 MC noise realizations for the conventional estimator $\hat{\mathcal{S}}_C$ for different true values $\mathcal{S}_0$ as a function of S/N: in the *canonical* case of the noise covariance matrix configuration ($\varepsilon_{eff} = 1$) – colored plain curves and in the *extreme* regime (ε_{eff} up to 2). The colored curves are shown from top to bottom in the same order as the legend lines on the right part of the figure. The low regime regions are invisible at the current plot scale and coincides with colored curves. The dashed line represents the "zero bias" level.

of angles in the range $[-\pi/2, \pi/2]$, their absolute difference is distributed uniformly in the range $[0, \pi/2]$. The root mean square of this distribution gives $\pi/\sqrt{12}$.

3. Bias analysis

In the following, the bias on $\mathcal{S}$ was calculated as follows:

$$Bias = \frac{1}{N_{MC}} \sum_{k=1}^{N_{MC}} \hat{\mathcal{S}}_{C,k} - \mathcal{S}_0 = \langle \hat{\mathcal{S}}_C \rangle - \mathcal{S}_0, \quad (15)$$

where $\hat{\mathcal{S}}_{C,k}$ is a realization of the conventional estimator of $\mathcal{S}$. We study different origins of the bias on $\hat{\mathcal{S}}_C$ by comparing the contributions of the biases due to the following parameters that affect its estimation: the true value $\mathcal{S}_0$ ($Bias_{\mathcal{S}_0}$), the shape of the noise covariance matrix ($Bias_{\mathcal{S}_0,\Sigma}$), the distribution of the true angles ($Bias_{\mathcal{S}_0,\psi_0}$) and the joint impact of these parameters ($Bias_{\mathcal{S}_0,\Sigma,\psi_0}$).

3.1. Impact of the true value $\mathcal{S}_0$

We calculated the average statistical bias induced by noise and the true value, $Bias_{\mathcal{S}_0}$, in the case with $\varepsilon_{eff} = 1$ and uniform configuration of the true angles. Figure 3 represents $Bias_{\mathcal{S}_0}$ (in colored plain curves) as a function of S/N, for values of $\mathcal{S}_0$ ranging from 0 to $\pi/2$ in steps of $\pi/16$ (11.25°). If the S/N is high, $\hat{\mathcal{S}}_C$ corresponds to $\mathcal{S}_0$, whereas if S/N is low, $\hat{\mathcal{S}}_C$ does not represent $\mathcal{S}_0$. The closer $\mathcal{S}_0$ to the bounds (0 or $\pi/2$), the larger the bias $Bias_{\mathcal{S}_0}$, even at high S/N ($p_0/\sigma_p > 10$). The largest bias occurs in the case where $\mathcal{S}_0 = 0$, which is the most remote value from $\pi/\sqrt{12}$ (where $\pi/\sqrt{12}$ is the result for $\hat{\mathcal{S}}_C$ if the orientation angles are random). Also, the conventional estimator $\hat{\mathcal{S}}_C$ can be ambiguous if it gives results close to $\pi/\sqrt{12}$.

In the presence of noise, $\hat{\mathcal{S}}_C$ is biased, though not necessarily positively biased, whereas the polarization fraction p is always positively biased (Montier et al. 2015a). For a true value of $\mathcal{S}_0$ lower than $\pi/\sqrt{12}$, the measured $\hat{\mathcal{S}}_C$ is positively biased, while it has negative bias for $\mathcal{S}_0$ larger than $\pi/\sqrt{12}$.

3.2. Impact of the (Q,U) effective ellipticity

Montier et al. (2015a) showed that the shape of the noise covariance matrix associated with a polarization measurement affects the bias on the polarization fraction p and angle ψ. Here we study the impact of the shape of the noise covariance matrix on the bias of the conventional estimator of the polarization angle dispersion function and evaluate under what conditions the assumption of non-correlated noise (i.e., $\varepsilon_{eff} = 1$) can be justified. For this purpose, we run the MC simulations as described in Sect. 2.2 in the three cases of the effective ellipticity and in the uniform configuration of the true angles.

We show in Fig. 3 the statistical bias of $\hat{\mathcal{S}}_C$ depending both on the true value and on the shape of the noise covariance matrix, $Bias_{\mathcal{S}_0,\Sigma}$, as a function of S/N and for different true values $\mathcal{S}_0$. In the *low* regime the shape of Σ_p has practically no effect on the bias: the corresponding dispersion can not be seen in the figure as it coincides with the *canonical* case curves. A dispersion in the initial bias $Bias_{\mathcal{S}_0}$ (corresonding to the amplitude of the gray areas) appears if there are important asymmetries in the shape of Σ_p, that is, in the *extreme* regime. We note that these asymmetries may either increase or decrease the statistical bias: $\langle \hat{\mathcal{S}}_C - \mathcal{S}_0 \rangle$ in the gray areas are higher or lower than the colored curves, that is, closer to or farther from the "zero bias" line, that occurs for $\pi/\sqrt{12}$ in the *canonical* case and shown by the dashed line in the

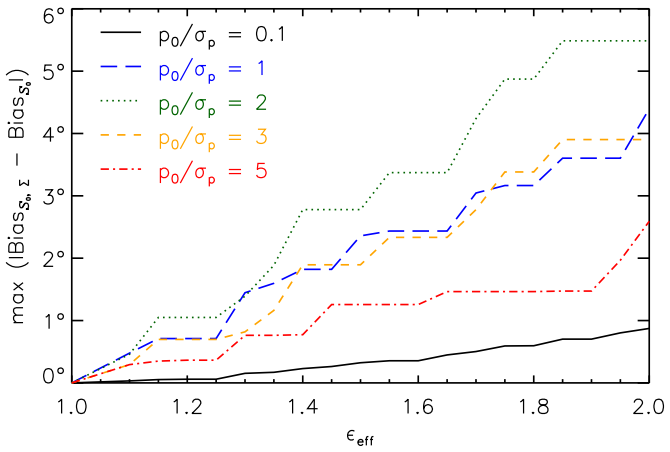

Fig. 4. Maximum absolute deviation of the bias induced by variations of the effective ellipticity between noise in (Q, U) and the true value $\mathcal{S}_0$, $Bias_{\mathcal{S}_{0,\Sigma}}$, from the bias induced by only the true value in the *canonical* case, $Bias_{\mathcal{S}_0}$ as a function of the effective ellipticity for different S/N.

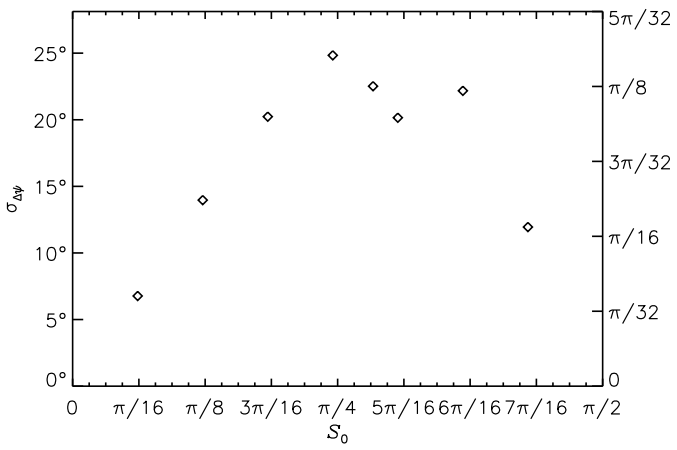

Fig. 5. Standard deviation of the difference between the true angle $\psi_{0,0}$ and the true angles $\psi_{0,i}$, $i \in [1, 9]$ as a function of the true polarization angle dispersion function $\mathcal{S}_0$ in the *canonical* case of the noise covariance matrix and random configuration of the true angles.

figure. If the true polarization angle dispersion function is close to $\pi/\sqrt{12}$, that is, close to the zero bias line, $Bias_{\mathcal{S}_{0,\Sigma}}$ is significant with respect to $Bias_{\mathcal{S}_0}$ (for $\mathcal{S}_0 = 3\pi/16$, $\pi/4$, $5\pi/16$, $3\pi/8$). If $\mathcal{S}_0$ is very different from $\pi/\sqrt{12}$, that is, remote from the zero bias line, both $Bias_{\mathcal{S}_0}$ and $Bias_{\mathcal{S}_{0,\Sigma}}$ become comparable for $S/N \geq 3$ (for $\mathcal{S}_0 = 0$, $\pi/16$, $\pi/8$, $7\pi/16$, $\pi/2$).

The dispersion in the bias $Bias_{\mathcal{S}_{0,\Sigma}}$ reaches its maximum at intermediate S/N ($p_0/\sigma_p \in [1, 3]$). At low S/N ($p_0/\sigma_p < 0.5$), there is almost no impact of the shape of the noise covariance matrix on the bias and we observe only the bias due to $\mathcal{S}_0$: the dispersion of $Bias_{\mathcal{S}_{0,\Sigma}}$ is much smaller than the level of $Bias_{\mathcal{S}_0}$. When the noise level is too high, it dominates any other effect. At high S/N, the noise level is low, so the estimation becomes accurate enough to become independent of the shape of the noise covariance matrix. Figure 4 shows the maximum absolute deviation of $Bias_{\mathcal{S}_{0,\Sigma}}$ from $Bias_{\mathcal{S}_0}$ over all possible values of $\mathcal{S}_0$ as a function of $\varepsilon_{\rm eff}$. The maximum deviation increases progressively with $\varepsilon_{\rm eff}$ and is the largest at $p_0/\sigma_p = 2$ with $\max(|\langle Bias_{\mathcal{S}_{0,\Sigma}} - Bias_{\mathcal{S}_0}\rangle|) = 5.3°$ ($\pi/34$).

Thus, the shape of the noise covariance matrix can significantly impact the bias on the polarization angle dispersion function. In the *extreme* regime and intermediate S/N, for the true values close to $\pi/\sqrt{12}$, the bias induced by the ellipticity and/or correlation between noise levels on Q and U is of the same order as the bias due to $\mathcal{S}_0$ in the *canonical* case (as for the values of $\mathcal{S}_0$ between $3\pi/16$ to $3\pi/8$ in Fig. 3): the width of the gray areas is comparable to the amplitude of the colored curves. Nevertheless, in the case where irregularities of the noise covariance matrix depart by less than 10% from the *canonical* case, that is, in the low regime, the impact of the asymmetry in the shape of the noise covariance matrix on the bias of $\hat{\mathcal{S}}_{\rm C}$ is negligible (the amplitude of the deviation from the bias in the *canonical* case $Bias_{\mathcal{S}_0}$ is very low and is not represented in the figure).

3.3. Impact of the true angles distribution

A multitude of different combinations of the true polarization angles $\psi_{0,i}$ can yield the same value $\mathcal{S}_0$. We study to which extent the polarization angle dispersion function can be affected by the configuration of the true angles. We compare the bias induced by the different configurations of the angles $Bias_{\mathcal{S}_0,\psi_0}$ to the bias due to the true value $Bias_{\mathcal{S}_0}$ in the uniform configuration (seen in Sect. 3.1). For this purpose, we performed simulations in the *canonical* case of the noise covariance matrix for the 10 simulated combinations of the true polarization angles in each of the configurations (random and uniform). Figure 5 shows the dispersion $\sigma_{\Delta\psi}$ of the differences between angles of the central pixel and of the neighbor pixels $\Delta\psi_{0,i}$ for $i \in [1, 9]$ as a function of $\mathcal{S}_0$ in the *canonical* case of the noise covariance matrix and the random configuration of the true angles. The dispersion of the angles that give the value $\mathcal{S}_0 = \pi/\sqrt{12}$ is also shown (the point between $\mathcal{S}_0 = \pi/4$ and $\mathcal{S}_0 = 5\pi/16$). We would like to point out that, by construction, random distributions of the true angles that give $\mathcal{S}_0 = 0$ and $\mathcal{S}_0 = \pi/2$ do not exist. Also, the closer $\mathcal{S}_0$ to these values (0 and $\pi/2$), the smaller the dispersion because there are less possible combinations of $\Delta\psi_{0,i}$.

In Fig. 6 we show the examples of the statistical bias $Bias_{\mathcal{S}_0,\psi_0}$ obtained in both configurations of the true angles. The different realizations of the uniform configuration in the *canonical* regime does not bring any contribution to the bias $Bias_{\mathcal{S}_0}$ obtained in the *canonical* case of the noise covariance matrix and fully reproduce the colored curves of Fig. 3. But when the distribution of the angles deviates from uniformity and becomes random, variations in the bias appear. In fact, each pair of angles $(\psi_{0,0}, \psi_{0,i})$ has its proper $\Delta\psi_{0,i} = \psi_{0,0} - \psi_{0,i}$ and only their mean squared sum gives $\mathcal{S}_0$. In the presence of noise, $\Delta\psi^2_{0,i}$ becomes biased. The sum of the biased quantities results in the dispersion of the total bias on $\hat{\mathcal{S}}_{\rm C}$.

Similarly to the case of the bias induced by both the true value and the shape of the noise covariance matrix $Bias_{\mathcal{S}_{0,\Sigma}}$, the dispersion in the bias due to the true value and the true angles distribution $Bias_{\mathcal{S}_0,\psi_0}$ increases at intermediate S/N and diminishes at low and high S/N, for the same reason discussed in Sect. 3.2 (gray areas become larger at intermediate S/N in Fig. 6). $\mathcal{S}_0 = \pi/4$ opens the widest range of possible $\Delta\psi_{0,i}$, ensuring the largest dispersion of values (Fig. 5). Thankfully, this value has a small bias due to $\mathcal{S}_0$: the corresponding colored curve in Fig. 6 is close to the zero bias level even at low S/N. At $p_0/\sigma_{\rm p} = 2$, the maximum dispersion of the bias for $\mathcal{S}_0 = \pi/4$ is almost 4° ($\simeq\pi/45$, corresponding to the width of the grey area) when the angles are distributed randomly, whereas the bias due only to noise is 0.8° ($\pi/225$).

In the *canonical* regime, the impact of the distribution of the angles used to calculate $\hat{\mathcal{S}}_{\rm C}$ can be of the order of few degrees

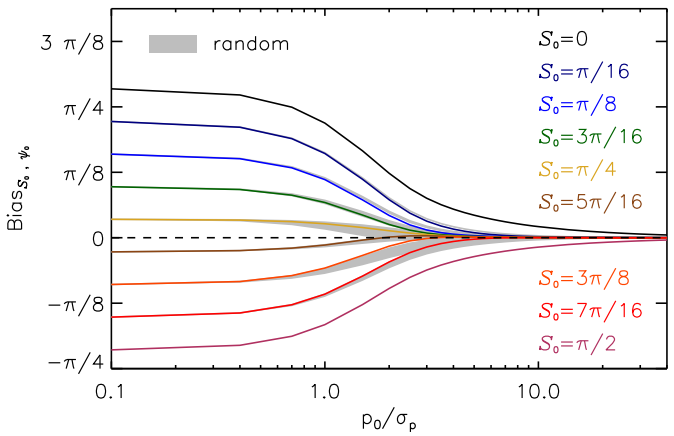

Fig. 6. Average bias on 10^6 MC noise simulations on $\hat{\mathcal{S}}_C$ in the uniform distribution of the true angles $\psi(\boldsymbol{x}+\boldsymbol{l}_i)$ (colored curves) and the dispersion of the average bias in the random distribution of the true angles (gray areas) in the *canonical* case of the noise covariance matrix ($\varepsilon_{\rm eff}=1$). The colored curves are shown from top to bottom in the same order as the legend lines on the right part of the figure. The dashed line represents the zero bias level.

in the worst case, that is, if the true angles are distributed quasi-randomly. However, in real observational data one would expect the polarization angles to be distributed neither uniformly nor randomly but within a particular structure in-between these two extreme configurations. The bias will increase with the number of pairs of angles $(\psi(\boldsymbol{x}), \psi(\boldsymbol{x}+\boldsymbol{l}_i))$ used for the computation of $\mathcal{S}$, that is, with the radius l, as reported by Serkowski (1958). The polarization angle structure function of Q and U obtained by Serkowski (1958) in the Perseus Double Cluster reached a limit when taking a radius larger than 12.8′ with 24 pairs of parameters taken into account.

In the *canonical* case of the noise covariance matrix, the impact of the true angles on the bias on $\hat{\mathcal{S}}_C$ can be neglected if a reasonable radius (or lag and width) with respect to the resolution of the data, is considered in the calculation. E.g., Planck Collaboration Int. XIX (2015) calculated the polarization angle dispersion function at a lag of 30′ with 30′ width which corresponds to 28 orientation angles at 1° degree resolution.

3.4. *Joint impact of the* (*Q*,*U*) ellipticity and of the distribution of the true angles

In this section, we study the simultaneous impact of the shape of the noise covariance matrix and of the distribution of the true angles on the estimation of $\hat{\mathcal{S}}_C$.

Montier et al. (2015a) showed that if the effective ellipticity between noise levels on Q and U differs from 1, then the bias on the polarization angle ψ oscillates depending on the true angle ψ_0. The period of the oscillations is about $\pi/2$ (see their Fig. 14). Thus, if there is a true difference $\Delta\psi_{0,i}=\pi/4$ between angles $\psi_0(\boldsymbol{x})$ and $\psi_0(\boldsymbol{x}+\boldsymbol{l}_i)$, their respective biases can maximize the total difference $\Delta\psi_i$ for some pairs. Note if the noise components on Q and U are correlated (i.e., $\rho\neq 0$), $\mathcal{S}_0=\pi/4$ will remain the value that yields the largest relative bias, while only the overall pattern would be shifted along ψ_0.

We run numerical simulations for the true value $\mathcal{S}_0=\pi/4$ that would maximize the bias between pairs of angles in the case $\varepsilon_{\rm eff}\neq 1$. We also explore $\mathcal{S}_0=\pi/8$ for illustration purposes. We show in Fig. 7 the average bias for the uniform and random configuration of the true angles in the *canonical*, low and *extreme* regimes. For $\varepsilon_{\rm eff}\neq 1$ (i.e., in the low and *extreme* regimes), the dispersion in the bias appears for both configurations, which is represented by the vertical width of the curves in the middle and bottom panels in Fig. 7. In the low regime, the uniform configuration of the true angles gives a dispersion that is lower than the dispersion in the random configuration for $\mathcal{S}_0=\pi/4$. However, in the *extreme* regime the situation is the opposite. This can be due to the fact that in the uniform configuration, the imposed $\mathcal{S}_0$ is valid for every pair of angles, thus

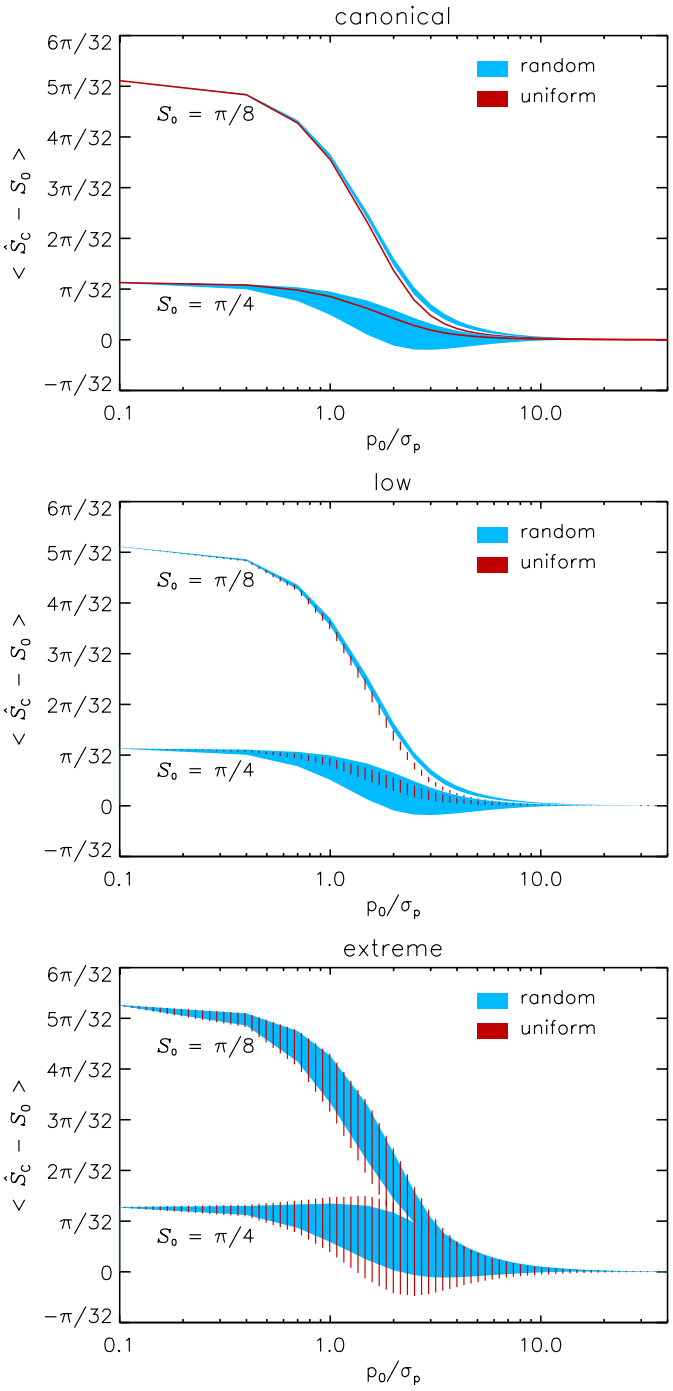

Fig. 7. Average bias on 10^6 MC realizations of the conventional estimator of the polarization angle dispersion function. Blue filled and red hashed areas delimit dispersion over 10 different sets of the true angles distributed randomly (blue) and uniformly (red) in three regimes of the shape of the noise covariance matrix, *from top to bottom*: canonical, low, extreme regimes.

giving $\Delta\psi_{0,i} = \mathcal{S}_0$, so that the relative bias between angles in a pair is maximized for some of the combinations. When angles are distributed randomly, $\mathcal{S}_0$ is ensured for the ensemble, but not for each pair: the pairs of angles with little relative bias diminish the final result. For $\mathcal{S}_0 = \pi/8$ and for other $\mathcal{S}_0 \neq \pi/4$ (not shown here), the observed difference between the random and uniform cases in the three regimes of $\varepsilon_{\rm eff}$ is less prominent than for $\mathcal{S}_0 = \pi/4$, but the overall behavior does not change.

The joint impact of the distribution of the true angles and the shape of the noise covariance matrix on the bias of $\hat{\mathcal{S}}_{\rm C}$ is high at intermediate S/N. In the *extreme* regime and in the uniform configuration, the dispersion in the bias with respect to the *canonical* case reaches its maximum of 10.1° ($\simeq\pi/18$) at $p_0/\sigma_{\rm p} = 2$. This is not far from the value of the dispersion due to variations of the effective ellipticity only, given by the width of the grey area for $\mathcal{S}_0 = \pi/4$ in Fig. 3 (8.9°, $\simeq\pi/20$). On the contrary, the dispersion in the bias in the random configuration gives only 6.4° ($\simeq\pi/28$) in the same S/N range. Thus, if the angles become random, it has little impact on the bias in the *extreme* regime. In the low regime and random configuration, the maximum dispersion in the bias is 4.2° ($\simeq\pi/43$) at $p_0/\sigma_p = 2$, while it is equal to 1.5° ($\pi/120$) in the uniform configuration. Such a behavior of the bias can have a particularly strong impact on the estimation of $\mathcal{S}$. If one considers a polarization pattern where angles become decorrelated with the distance, so that close to the pixel of interest, angles are more or less similar and they become random with the distance. In that case, the angles close to the pixel for which the polarization angle dispersion function is calculated, will be affected more by the bias (positive or negative) due to the distribution of true angles than those which are farther. This would lead to a non-homogeneity in the estimation of the polarization angle dispersion function in both low and *extreme* regimes of the noise covariance matrix. Such an issue will not arise if one considers the polarization angle dispersion function calculated at a given lag, $\mathcal{S}(\boldsymbol{x}, l, \delta)$, and if the width of the annulus is small compared to the typical scale for decorrelation of angles

3.5. Conventional uncertainties

As soon as the uncertainties of each of the angles $\psi(\boldsymbol{x})$ and $\psi(\boldsymbol{x} + \boldsymbol{l}_i)$ can be derived, one can obtain an estimate of the uncertainty on $\hat{\mathcal{S}}_{\rm C}$ using the partial derivatives method. Such an estimator of the uncertainty will be called the "conventional" estimator hereafter. The conventional uncertainty of $\hat{\mathcal{S}}_{\rm C}$ is given by (see Appendix A for derivation):

$$\sigma_{\mathcal{S},\rm C} = \frac{1}{N\mathcal{S}(\boldsymbol{x}, l)} \left[\left(\sum_{i=1}^{N} [\psi(\boldsymbol{x}) - \psi(\boldsymbol{x} + \boldsymbol{l}_i)] \right)^2 \sigma^2_{\psi(\boldsymbol{x})} \right. \tag{16}$$

$$\left. + \sum_{i=1}^{N} [\psi(\boldsymbol{x}) - \psi(\boldsymbol{x} + \boldsymbol{l}_i)]^2 \sigma^2_{\psi(\boldsymbol{x}+\boldsymbol{l}_i)} \right]^{1/2}. \tag{17}$$

Although the conventional method is limited to relatively high S/Ns to ensure small deviations from the true value, it is the easiest method to derive an uncertainty on $\hat{\mathcal{S}}_{\rm C}$ once the data and the associated noise information for each component are available. In order to quantify to which extent the conventional uncertainty can be reliable, we compare it to the uncertainty on $\hat{\mathcal{S}}_{\rm C}$ given by the standard deviation of the distribution, denoted by $\sigma_{\mathcal{S},0}$. The ratio of these uncertainties is shown in Fig. 8 in the *canonical*, low, and *extreme* regimes. Uncertainties on the angles, $\sigma^2_{\psi(\boldsymbol{x})}$, $\sigma^2_{\psi(\boldsymbol{x}+\boldsymbol{l}_i)}$, used in the determination of $\sigma_{\mathcal{S},\rm C}$, are also calculated

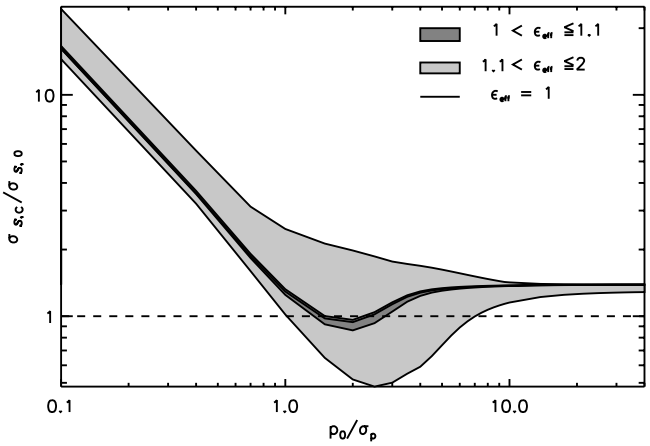

Fig. 8. Ratio between the conventional uncertainty and the true uncertainty of polarization angle dispersion function for different configurations of the noise covariance matrix. The dashed line represents the value of 1.

by the conventional method (Montier et al. 2015a) using Q and U and noise covariance matrices $\Sigma_{p,i}$ of each pixel. Then, one should note that $\sigma_{\psi(\boldsymbol{x})}$ and $\sigma_{\psi(\boldsymbol{x}+\boldsymbol{l}_i)}$ are themselves subject to the limitation of the derivatives method.

At low S/N ($p_0/\sigma_p < 1$), the estimate of the uncertainty using the conventional method is very inaccurate. In the *canonical* case of the noise covariance matrix, $\sigma_{\mathcal{S},\rm C}$ rapidly converges toward the true uncertainty and becomes compatible within 10% in the range $p_0/\sigma_p \in [1, 3]$. Then it increases at higher S/N and overestimates the uncertainty on polarization angle dispersion function up to 38% at high (larger than 20) S/N of p. The ratio does not converge to 1 at high S/Ns. In the case of more complex shapes of the noise covariance matrix, $\sigma_{\mathcal{S},\rm C}$ can deviate from the true value by a factor of two at S/Ns ranging between 1 and 10. At S/N larger than 10, the ellipticity and correlation between Q and U do not affect the estimation of the uncertainty and $\sigma_{\mathcal{S},\rm C}$ becomes equal to that in the *canonical* regime.

The uncertainty on the polarization angle dispersion function determined by the conventional method can be used at S/N larger than one in the *canonical* case of the noise covariance matrix and gives a very conservative estimate of the true uncertainty.

4. Other estimators

4.1. Dichotomic estimator

The bias on the polarization angle dispersion function occurs because of the non-linearity in the Eq. (5) when deriving $\hat{\mathcal{S}}_{\rm C}$ from the Stokes parameters. In order to overcome this issue, one can use the dichotomic estimator that consists of combining two independent measurements of the same quantity. The square of the dichotomic estimator of the polarization angle dispersion function has the following form:

$$\hat{\mathcal{S}}^2_{\rm D}(\boldsymbol{x}, l) = \frac{1}{N(l)} \sum_{i=1}^{N(l)} [\psi_1(\boldsymbol{x}) - \psi_1(\boldsymbol{x} + \boldsymbol{l}_i)] \left[(\psi_2(\boldsymbol{x}) - \psi_2(\boldsymbol{x} + \boldsymbol{l}_i)) \right], \tag{18}$$

where subscripts 1 and 2 correspond respectively to each of the two data sets. We simulated the behavior of the dichotomic estimator of $\mathcal{S}^2$ by assuming the noise level of the two data sets to

be $\sqrt{2}$ times lower than the noise level considered for the conventional estimator $\hat{\mathcal{S}}_{\rm C}$. This allowed us to reproduce the situation where the original data had been divided in two subsets, so that $\sigma_{\rm p}$ becomes $\sqrt{2}\,\sigma_{\rm p}$ (as in the case of the *Planck* satellite data). The true angles were considered to be in the uniform configuration and the noise covariance matrix was in the *canonical* regime. Figure 9 shows the examples of the DFs of $\hat{\mathcal{S}}_{\rm D}^2$ for $\mathcal{S}_0 = \pi/8$ and $\mathcal{S}_0 = 3\pi/8$. At low S/Ns, the mean estimate of the DFs, $\langle \hat{\mathcal{S}}_{\rm D}^{\,2} \rangle$ tends to 0. The same trend is observed for any $\mathcal{S}_0$. The average bias for different values of $\mathcal{S}_0$ is shown in Fig. 10. We conclude that the dichotomic estimator of the polarization angle dispersion function is always negatively biased.

The dichotomic estimator $\hat{\mathcal{S}}_{\rm D}^2$ is not suitable for accurate estimate of the polarization angle dispersion function because it is a quadratic function that can take negative values. However, as its behavior is opposite to that of $\hat{\mathcal{S}}_{\rm C}$ in the range $\mathcal{S}_0 \in [0, \pi/\sqrt{12}]$, it can be used as a verification of the validity of $\hat{\mathcal{S}}_{\rm C}$:

- if $\hat{\mathcal{S}}_{\rm C} > \pi/\sqrt{12}$ and $\hat{\mathcal{S}}_{\rm D}^2 > \pi^2/12$, then the noise level is low, $\mathcal{S}_0$ is larger than $\pi/\sqrt{12}$, and $\hat{\mathcal{S}}_{\rm C}$ gives a reliable estimate of $\mathcal{S}_0$;
- if $\hat{\mathcal{S}}_{\rm C} > \pi/\sqrt{12}$ and $\hat{\mathcal{S}}_{\rm D}^2 < \pi^2/12$, then the noise level is high and $\mathcal{S}_0$ is probably larger than $\pi/\sqrt{12}$. In this case we suggest to estimate the upper limit of the bias as described in Sect. 4.4;
- if $\hat{\mathcal{S}}_{\rm C} < \pi/\sqrt{12}$ and $\hat{\mathcal{S}}_{\rm D}^2 < \pi^2/12$, then $\mathcal{S}_0$ is smaller than $\pi/\sqrt{12}$. We propose to use a polynomial combination of both $\hat{\mathcal{S}}_{\rm C}^{\,2}$ and $\hat{\mathcal{S}}_{\rm D}^2$ to better estimate $\mathcal{S}$ (see Sect. 4.3) if two independent data sets are available, or to estimate the upper limit of the bias as described in Sect. 4.4.

4.2. Bayesian DFs of $\mathcal{S}$

In an attempt to develop an accurate estimator of the polarization angle dispersion function, we use the difference between the behaviors of the conventional and dichotomic estimators in the range $\mathcal{S}_0 \in [0, \pi/\sqrt{12}]$. In order to obtain $\mathcal{S}_0$ knowing $\hat{\mathcal{S}}_{\rm C}$ and $\hat{\mathcal{S}}_{\rm D}^2$ from the data, we use the Bayes' theorem. The posterior DF of $\mathcal{S}_0$ can be given by

$$D(\mathcal{S}_0|\hat{\mathcal{S}}_{\rm C}^{\,2}, \hat{\mathcal{S}}_{\rm D}^{\,2}, \Sigma) = \frac{g(\hat{\mathcal{S}}_{\rm C}^{\,2}, \hat{\mathcal{S}}_{\rm D}^{\,2}|\mathcal{S}_0, \Sigma) k(\mathcal{S}_0)}{\int_0^{\pi/2} g(\hat{\mathcal{S}}_{\rm C}^{\,\prime 2}, \hat{\mathcal{S}}_{\rm D}^{\,\prime 2}|\mathcal{S}_0', \Sigma) k(\mathcal{S}_0') {\rm d}\mathcal{S}_0'}, \qquad (19)$$

where $k(\mathcal{S}_0)$ is a prior on $\mathcal{S}_0$, which we choose to be flat in the range $[0, \pi/2]$. Here, $g(\hat{\mathcal{S}}_{\rm C}^{\,2}, \hat{\mathcal{S}}_{\rm D}^{\,2}|\mathcal{S}_0, \Sigma)$ is the distribution function of the conventional and dichotomic estimators knowing the true polarization angle dispersion function $\mathcal{S}_0$ and the noise covariance matrix.

We numerically built the posterior DFs $D(\mathcal{S}_0|\hat{\mathcal{S}}_{\rm C}^{\,2}, \hat{\mathcal{S}}_{\rm D}^{\,2}, \Sigma)$ for different values of $\mathcal{S}_0$ and different S/N in the *canonical* regime. For this purpose, we first defined a two-dimensional grid G of the size $N_{\rm c} \times N_{\rm d}$ where $N_{\rm c}$ and $N_{\rm d}$ are the numbers of sampling of the squared conventional and dichotomic estimators in the ranges $[0, (\pi/2)^2]$ and $[-(\pi/2)^2, (\pi/2)^2]$, respectively. $N_{\rm c}$ and $N_{\rm d}$ were chosen in a way to make sure that the meshes of the grid are squares with the size of 0.00826 rad^2 ($N_{\rm c} = 300$, $N_{\rm d} = 600$). Second, we run MC simulations for $\mathcal{S}_0 \in [0, \pi/2]$ as previously. For each $\mathcal{S}_0$ we performed $N_{\rm MC} = 10^6$ noise realizations in the *canonical* case of the noise covariance matrix, giving

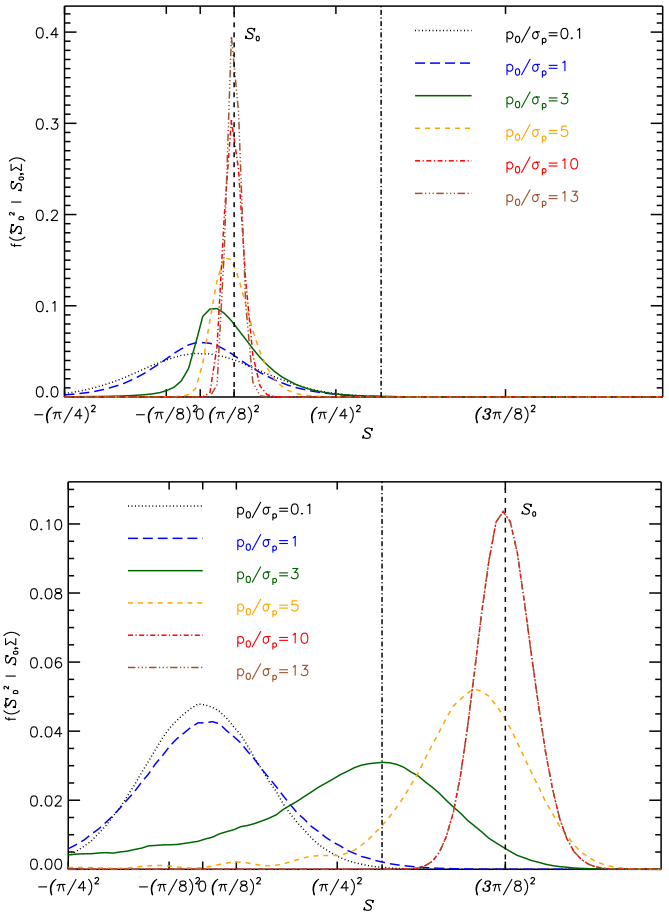

Fig. 9. Examples of the distribution function of the dichotomic estimator $\hat{\mathcal{S}}_{\rm D}^2$ in the *canonical* regime ($\varepsilon_{\rm eff} = 1$). *Top*: $\mathcal{S}_0 = \pi/8$. *Bottom*: $\mathcal{S}_0 = 3\pi/8$. Note squared values. The vertical dashed line shows the true value and the vertical dash-dotted line shows the value of $\pi^2/12$.

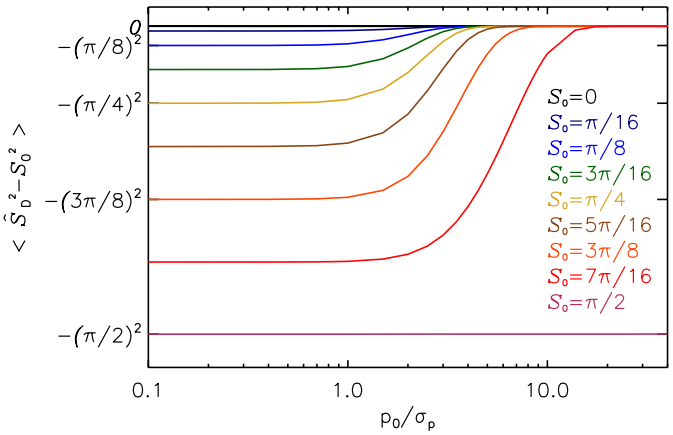

Fig. 10. Average bias on 10^6 MC realizations of the dichotomic estimator $\hat{\mathcal{S}}_{\rm D}^2$ in the *canonical* case of the noise covariance matrix: $\varepsilon_{\rm eff} = 1$ for the true values of $\mathcal{S}_0$ varying between 0 and $\pi/2$ as a function of S/N. The colored curves are shown from top to bottom in the same order as the legend lines on the right part of the figure.

$N_{\rm MC}$ pairs of $(\hat{\mathcal{S}}_{{\rm C}k}^{\,2}, \hat{\mathcal{S}}_{{\rm D}k}^{\,2})_k$, where $k \in [1, N_{\rm MC}]$. After each run k, the corresponding $\mathcal{S}_0$ was attributed to the mesh of the grid with coordinates $(\hat{\mathcal{S}}_{{\rm C}k}^{\,2}, \hat{\mathcal{S}}_{{\rm D}k}^{\,2})_k$. Finally, we averaged over $\mathcal{S}_0$ in each mesh and obtain a grid of $\bar{\mathcal{S}}_0$.

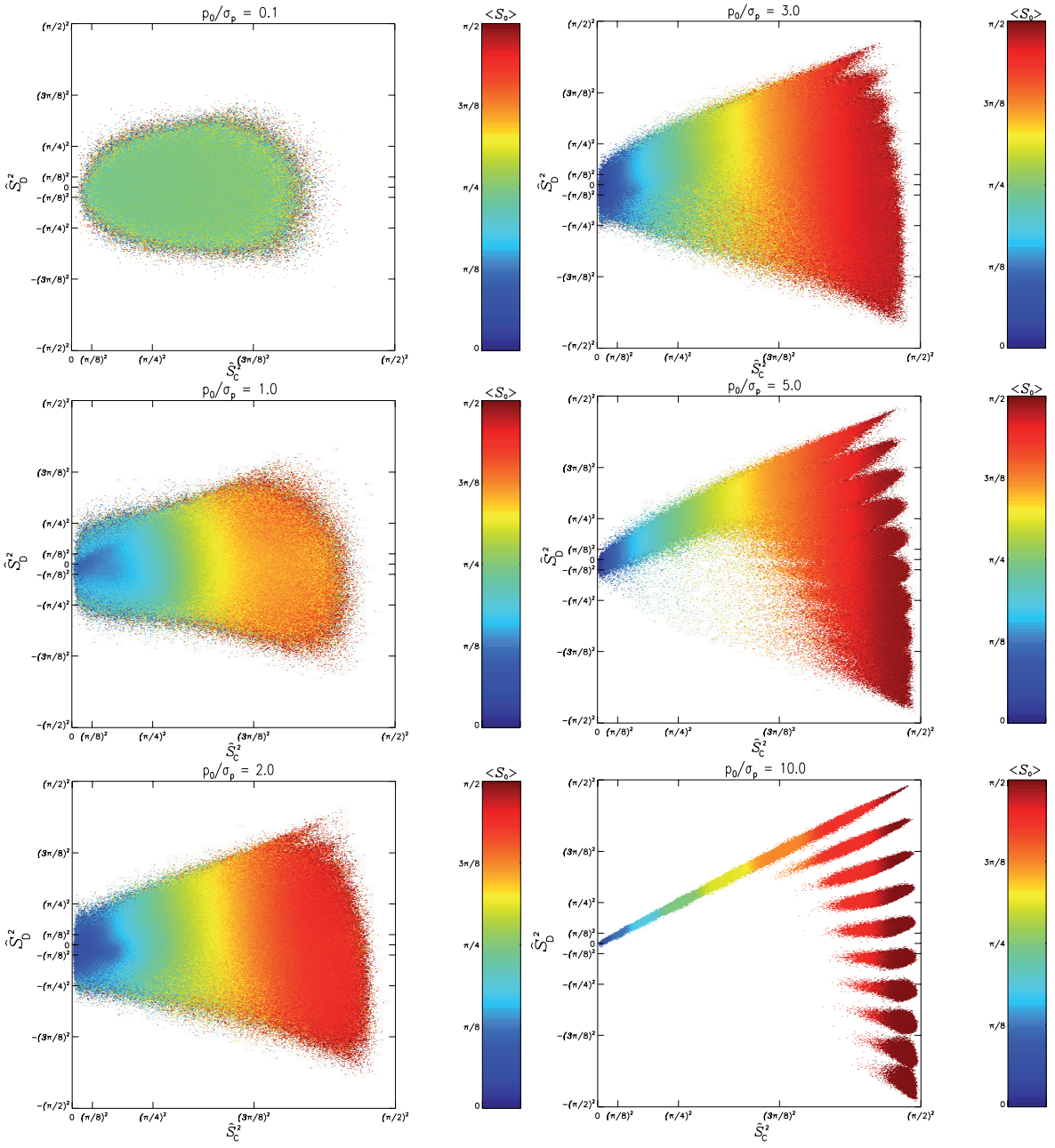

Fig. 11. Average of $\mathcal{S}_0$ over the posterior distribution functions of $D(\mathcal{S}_0|\hat{\mathcal{S}_C}^2, \hat{\mathcal{S}_D}^2, \Sigma)$ for p_0/σ_p = 0.1, 1, 2 (*left column, from top to bottom*) and 3, 5, 10 (*right column, from top to bottom*) simulated in the *canonical* case of the noise covariance matrix.

Examples of $\bar{\mathcal{S}}_0$ for different S/Ns in the *canonical* case of Σ_p are shown in Fig. 11. We note that, at very low S/N (top left panel) almost all combinations of the two estimators give $\bar{\mathcal{S}}_0$ distributed around $\pi/4$. Because of the noise, both estimators fail to correctly estimate $\mathcal{S}_0$ and all possible $\mathcal{S}_0 \in [0, \pi/2]$ give $\pi/4$ on average. But already at $p_0/\sigma_p = 1$ (middle left panel), there is a correlation between $\hat{\mathcal{S}_C}^2$ and $\bar{\mathcal{S}}_0$ and small variations of $\bar{\mathcal{S}}_0$ with $\hat{\mathcal{S}_D}^2$ appear. At intermediate S/N ($p_0/\sigma_p = 2$, 3, bottom left and top right panels respectively) the dependence of $\bar{\mathcal{S}}_0$ on $\hat{\mathcal{S}_C}^2$ is the most marked: $\bar{\mathcal{S}}_0$ is correlated with $\hat{\mathcal{S}_C}^2$ for any $\hat{\mathcal{S}_D}^2$. In fact, as the posterior approach forces $\bar{\mathcal{S}}_0$ to be positive, and as $\hat{\mathcal{S}_C}$ is positive by definition, this explains that $\bar{\mathcal{S}}_0$ depends strongly on the conventional estimator. Also, high-value $\hat{\mathcal{S}_D}^2$ are difficult to obtain at low and intermediate S/N as it tends to 0 in presence of noise. On the contrary, the dependence of $\bar{\mathcal{S}}_0$ on the dichotomic estimator is stronger at low $|\hat{\mathcal{S}_D}^2|$ and low $\hat{\mathcal{S}_C}^2$ (dark blue to light blue variations in panels corresponding to p_0/σ_p = 1, 2, 3). At higher S/N ($p_0/\sigma_p > 5$, center and bottom right panels), there is a strong correlation of $\bar{\mathcal{S}}_0$ with both $\hat{\mathcal{S}_C}^2$ and $\hat{\mathcal{S}_D}^2$. At these S/N, $\hat{\mathcal{S}_D}^2$ takes positive values for moderate $\mathcal{S}_0$, but as soon as $\mathcal{S}_0$ approaches $\pi/2$, $\hat{\mathcal{S}_D}^2$ is not efficient and we observe a feather-like pattern. We note that some values of $\hat{\mathcal{S}_C}^2$ and $\hat{\mathcal{S}_D}^2$ are never reached, or, in other words, there are values of $\hat{\mathcal{S}_C}$ and $\hat{\mathcal{S}_D}^2$ which do not give any $\bar{\mathcal{S}}_0$. We would like to emphasize that the empirical Bayesian approach used here never gives 0 even at low $(\hat{\mathcal{S}_C}, \hat{\mathcal{S}_D}^2)$ as this method averages over the values defined between 0 and $\pi/2$.

4.3. Polynomial estimator

In order to be able to directly use the conventional and dichotomic estimators of $\mathcal{S}^2$, without computing the Bayesian Posterior DFs, we search for a polynomial combination of $\hat{\mathcal{S}_{\rm C}}^2$ and $\hat{\mathcal{S}_{\rm D}}^2$ which would reflect the above simulations. To do so, we fitted the surface $\bar{\mathcal{S}}_0$ by a polynomial of the following form:

$$\hat{\mathcal{S}}_P = \sum C_{a,b,n} \left(\hat{\mathcal{S}_{\rm C}}^2\right)^a \left(\hat{\mathcal{S}_{\rm D}}^2\right)^b, \tag{20}$$

where $a \in [0, n]$, $b \in [0, n]$ and n is the order of the polynomial. Thus, for each S/N and a given order, one would have the corresponding coefficients $C_{a,b,n}$. By applying these coefficients to any couple $(\hat{\mathcal{S}_{\rm C}}^2, \hat{\mathcal{S}_{\rm D}}^2)$ at a given S/N, one should be able to obtain the polynomial estimator $\hat{\mathcal{S}}_P$.

Polynomial orders from 1 to 6 have been tested via comparison of the estimator $\hat{\mathcal{S}}_P$ to the result of the simulations $\bar{\mathcal{S}}_0$. We focused on the case of the intermediate S/N ($p_0/\sigma_p = 2$), as it corresponds to the regime where the bias on $\hat{\mathcal{S}}_{\rm C}$ is the most affected by irregularities in the shape of $\Sigma_{\rm p}$. The polynomial order 4 is the best compromise between the order of the polynomial degree and the goodness of the fit.

Once $C_{a,b,n}$ are known, one can apply them to any couple of the measured estimators $(\hat{\mathcal{S}_{\rm C}}^2, \hat{\mathcal{S}_{\rm D}}^2)$ in order to calculate the polynomial estimator. Nonetheless, one should be cautious about unrealistic values such as low $\hat{\mathcal{S}_{\rm C}}^2$ and high $|\hat{\mathcal{S}_{\rm D}}^2|$, where no correct result can exist.

The average biases of the polynomial and conventional estimators in the *canonical* regime and uniform configuration of the true angles are compared in Fig. 12 for different S/Ns and $\mathcal{S}_0$. In the range $\mathcal{S}_0 \in [0, \pi/\sqrt{12}]$, the conventional estimator biases positively, while the dichotomic one negatively: their contributions are opposite, and $\hat{\mathcal{S}}_P$ gives more reliable results and performs better than $\hat{\mathcal{S}}_{\rm C}$ at low and intermediate S/Ns. For example, at $p_0/\sigma_p = 2$, the bias on $\hat{\mathcal{S}}_P$ is as high as 88% of the bias on $\hat{\mathcal{S}}_{\rm C}$ at $\mathcal{S}_0 = 0$ and it vanishes completely towards $\mathcal{S}_0 = \pi/4$. Beyond the S/N of 4, the polynomial estimator is less accurate than the conventional one. For $\mathcal{S}_0 \in [\pi/\sqrt{12}, \pi/2]$, the bias for both conventional and dichotomic estimators is negative and $\hat{\mathcal{S}}_P$ fails compared to the conventional estimator, as expected.

In this study, contributions of $\hat{\mathcal{S}}_{\rm C}$ and $\hat{\mathcal{S}}_{\rm D}$ have been supposed to be equal, because $\mathcal{S}_0$ is not known a priori. As a step forward, one can iterate on priors on $\hat{\mathcal{S}}_{\rm C}$ and $\hat{\mathcal{S}}_{\rm D}$ in order to improve the estimation of $\mathcal{S}_0$. When the first approximate result is obtained and the tendency with respect to high/low $\mathcal{S}_0$ is recognized, one could attribute more or less weight to the estimator that is effective in that range of $\mathcal{S}_0$.

4.4. Estimation of the upper limit of the bias on $\hat{\mathcal{S}}_C$

When the dichotomic estimator cannot be calculated, that is, there is only one measurement per spatial position, it is helpful to evaluate to which extent one can trust the conventional estimator, given by Eq. (5). We propose a simple test that consists of calculating the maximum bias due to the noise of the data.

As seen in Sect. 3, the largest bias occurs for $\mathcal{S}_0 = 0$. A MC noise simulation consistent with the noise covariance matrices of the data at $\mathcal{S}_0 = 0$ would give the value of the maximum possible bias. For that purpose we need to change I, Q and U in such a manner as to have $\mathcal{S}_0 = 0$, and we keep the S/N of p unchanged. The only way to have $\mathcal{S}_0 = 0$ is to attribute the same

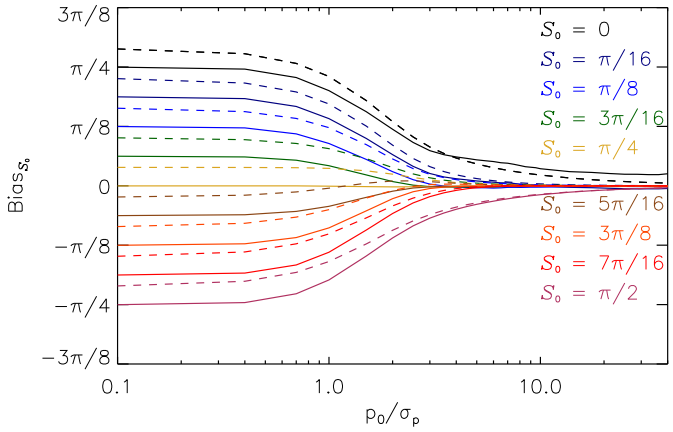

Fig. 12. Average bias on 10^6 MC realizations on conventional (dashed curves) and polynomial (plain curves) estimators in the *canonical* case of covariance matrix ($\varepsilon_{\rm eff} = 1$) for various $\mathcal{S}_0$ as a function of p_0/σ_p. The colored curves are shown from top to bottom in the same order as the legend lines on the right part of the figure.

true polarization angle for all the pixels inside the considered area. Such a configuration is given by

$$\frac{\widetilde{U}}{\widetilde{Q}} = r, \tag{21}$$

where r is a real constant, $\widetilde{U}$ and $\widetilde{Q}$ are the Stokes parameters which will be used in the calculation of the upper limit on the bias on the polarization angle dispersion function. The total intensity should also be modified in order to preserve p. It is given by

$$\widetilde{I} = \frac{\sqrt{\widetilde{Q}^2(1+r^2)}}{p}. \tag{22}$$

The system for $(\widetilde{I}, \widetilde{Q}, \widetilde{U})$ can be closed if we adopt an expression for $\sigma_{\rm p}$. We consider $\sigma_{\rm p}$ as given by the conventional uncertainty estimator with no cross-correlation terms:

$$\sigma_{\rm p} = \frac{\sqrt{Q^2\sigma_Q^2 + U^2\sigma_U^2 + p^4 I^2 \sigma_I^2}}{pI^2}. \tag{23}$$

Then, the new Stokes Q parameter is given by

$$\widetilde{Q} = \frac{p\sqrt{\sigma_Q^2 + r^2\sigma_U^2 + p^2(1+r^2)\sigma_I^2}}{(1+r^2)\sigma_{\rm p}}, \tag{24}$$

and the expression of the new Stokes U parameter is the following:

$$\widetilde{U} = r\,\widetilde{Q}. \tag{25}$$

For example, we took the true value $\mathcal{S}_0 = 22.5°$ in the uniform configuration of the true angles and the effective ellipticity $\varepsilon_{\rm eff} = 1.1$ (low regime) with $\varepsilon = 1.1$ and $\rho = 0$. We assumed the total intensity I_0 to be equal to 1 and perfectly known as in the above simulations, so that we dealt with the reduced noise covariance matrix (see Eq. (11). We also assumed the uncertainty $\sigma_U = U_0$, then $\sigma_Q = \varepsilon\sigma_U = 1.1\sigma_U$ from Eq. (10). This allowed us to build the simulated noise covariance matrix $\Sigma_{\rm p}$. We simulated a measurement by running one noise realization consistent with $\Sigma_{\rm p}$

and obtained $\hat{\mathcal{S}}_C = 43.1°$. We followed the above-described procedure and, averaging over 10^6 noise realizations we obtained the mean value of the maximum bias $\langle Bias_{\max} \rangle = 21.5°$ with the standard deviation $\sigma(Bias_{\max}) = 7.5°$. Thus, in this case, the estimation of $\mathcal{S}$ can be affected by bias almost by the same order of magnitude as the true value. This method can not be directly used to "de-bias" the conventional estimator but can be used to estimate, on average, at which level the estimation of the polarization angle dispersion function is affected by the noise level and the shape of the noise covariance matrix.

5. Discussion and conclusion

In this paper, we studied the bias on the polarization angle dispersion function and we have demonstrated its complex behavior for the first time. We showed that it strongly depends on the true value which is not known a priori: the bias on the conventional estimator is negative for $\mathcal{S}_0 > \pi/\sqrt{12}$ ($\simeq 52°$), which is the value corresponding to the result if all the angles considered in the calculation are random, positive for $\mathcal{S}_0 < \pi/\sqrt{12}$, and it can reach up to $\pi/\sqrt{12}$ at low S/Ns (Sect. 3.1). The bias on the polarization angle dispersion function also depends on the shape of the noise covariance matrix and the distribution of the true angles in the intermediate range of S/N, between 1 and 4 as seen in Sects. 3.2, 3.3. However, if there is less than 10% effective ellipticity between noise levels on Stokes parameters Q and U, the impact of the shape of the noise covariance matrix and of the distribution of the true angles can be neglected. Otherwise, these factors can significantly affect the estimation of the polarization angle dispersion function when using the conventional estimator.

We have introduced the dichotomic estimator of $\mathcal{S}$ and studied its behavior. We showed that the bias on $\hat{\mathcal{S}}_D^2$ is always negative. In addition, such an estimator has the disadvantage of being a quadratic function that can take negative values. However, using both conventional and dichotomic estimators appears to be the first step in assessing the true value of the polarization angle dispersion function. We have introduced a new polynomial estimator that allows us to use the low S/N data (less than 4). This broadens the application of the polarization angle dispersion function in different polarimetric studies. Yet deriving the polynomial estimator requires the existence of at least two independent measurements as well as an additional computational time to run simulations.

We propose a method to evaluate the maximum possible bias of the polarization angle dispersion function knowing the noise covariance matrix of the data. It can be used as an estimator of the upper limit to the bias on $\hat{\mathcal{S}}_C$ with any polarimetric data with the available noise covariance matrices in (Q, U).

The methods developed in this work (maximum bias estimation and dichotomic estimator) have been applied to the *Planck* data in order to analyze the observed dust polarization with respect to the magnetic field structure. Planck Collaboration Int. XIX (2015) calculates the polarization angle dispersion function in an annulus of a 30′ lag and 30′ width all over the sky at 1° resolution, revealing filamentary features. Using the dichotomic estimator and the test of the maximum bias on $\mathcal{S}$, Planck Collaboration Int. XIX (2015) demonstrates that these filamentary features are not artifacts of noise. Moreover, a clear anti-correlation between the polarization fraction and the polarization angle dispersion function has been shown.

Planck Collaboration Int. XIX (2015) uses the data smoothed to 1° resolution, which diminishes the noise level. Also, as the effective ellipticity of the *Planck* data deviates at most by 12% from the *canonical* case (Planck Collaboration Int. XIX 2015), the shape of the noise covariance matrix has been taken into account in the estimation of $\mathcal{S}$. The results of this work can also be particularly well suited in the analysis of the data from the new experiments that are designed for polarized emission studies, such as the balloon-borne experiments BLAST-Pol (Fissel et al. 2010), PILOT (Bernard et al. 2007) and the ground-based telescopes with new polarization capabilities: ALMA (Pérez-Sánchez & Vlemmings 2013), SMA, NIKA2 (Catalano et al. 2016). We suggest to calculate both the conventional and dichotomic estimators in order to compare both, in the case where two independent data-sets are available, as well as to estimate the upper limit of the bias on $\mathcal{S}$ using the method proposed in this work for any polarimetric data with the noise covariance matrix provided. A joint IDL/Python library which includes the methods from the work on bias analysis and estimators of polarization parameters is currently under development.

References

Andersson, B.-G., Lazarian, A., & Vaillancourt, J. 2015, ARA&A, 53, 501
Beck, R., & Gaensler, B. 2004, New Astron. Rev., 48, 1289
Benoît, A., Ade, P., Amblard, A., et al. 2004, A&A, 424, 571
Bernard, J.-P., Ade, P., De Bernardis, P., et al. 2007, EAS Pub. Ser., 23, 189
Catalano, A., Adam, R., Ade, P., et al. 2016, ApJ, submitted [arXiv:1605.08628]
Chandrasekhar, S., & Fermi, E. 1953, ApJ, 118, 113
Cortes, P., Girart, J., Hull, C., et al. 2016, ApJ, 825, 15
Crutcher, R., Nutter, D., Ward-Thompson, D., & Kirk, J. 2004, ApJ, 600
Davis, L., & Greenstein, J. 1951, ApJ, 114, 206
Dotson, J., Vaillancourt, J., Kirby, L., Dowell, C., & Hildebrand, R. 2010, ApJ, 186, 406
Falceta-Gonçalves, D., Lazarian, A., & Kowal, G. 2008, ApJ, 679, 537
Fissel, L. M., Ade, P. A. R., Angilé, F. E., et al. 2010, in Proc. SPIE, 7741
Fletcher, A. 2010, in ASP Conf. Ser. 438, eds. R. Kothes, T. Landecker, & A. Willis, 197
Girart, J. M., Rao, R., & Marrone, D. P. 2006, Science, 313, 812
Hall, J., & Mikesell, A. 1949, AJ, 54, 187
Han, J. 2002, Chin. J. Astron. Astrophys., 2, 293
Heiles, C. 1996, ApJ, 462, 316
Heiles, C., & Troland, T. 2005, ApJ, 624, 773
Hildebrand, R., Kirby, L., Dotson, J., Houde, M., & Vaillancourt, J. 2009, ApJ, 696, 567
Hiltner, W. 1949, ApJ, 109, 471
Hiltner, W. 1951, ApJ, 114, 241
Houde, M., Rao, R., Vaillancourt, J., & Hildebrand, R. 2011a, ApJ, 733, 109
Houde, M., Vaillancourt, J., Hildebrand, R., Chitsazzadech, S., & Kirby, L. 2011b, ApJ, 706, 1504
Houde, M., Hull, C., Plambeck, R., Vaillancourt, J., & Hildebrand, R. 2016, ApJ, 820, 38
Lai, S.-P., Crutcher, R. M., & Girart, J. M. 2001, BAAS, 33, 1360
Lazarian, A., & Hoang, T. 2008, ApJ, 676, L25
Mao, S., Gaensler, B., Haverkorn, M., et al. 2010, ApJ, 714, 1170
Mathewson, D., & Ford, V. 1970, MmRAS, 74, 139
Matthews, B., McPhee, C., Fisse, L., & Curran, R. 2009, ApJ, 182, 143
Montier, L., Plaszczynski, S., Levrier, F., et al. 2015a, A&A, 574, A135
Montier, L., Plaszczynski, S., Levrier, F., et al. 2015b, A&A, 574, A136
Pérez-Sánchez, A., & Vlemmings, W. 2013, A&A, 551, A15
Planck Collaboration Int. XIX. 2015, A&A, 576, A104
Poidevin, F., Bastien, P., & Matthews, B. 2010, ApJ, 716, 893
Quinn, J. 2012, A&A, 538, A65
Sandstrom, K. M., Latham, D. W., Torres, G., Landsman, W. B., & Stefanik, R. P. 2002, BAAS, 34, 1300
Serkowski, K. 1958, Acta Astron., 8, 135
Simmons, J., & Stewart, B. 1985, A&A, 142, 100
Tang, Y.-W., Ho, P., Koch, P., Guilloteau, S., & Dutrey, A. 2012, Proc. Magnetic Fields in the Universe
Vaillancourt, J. 2007, EAS Pub. Ser., 23, 147
Vaillancourt, J. E. 2006, PASP, 118, 1340
Wardle, J., & Kronberg, P. 1974, ApJ, 194, 249
Zhang, Q., Qiu, K., Girart, J., et al. 2010, PASP, 792, 116

Appendix A: Derivation of the conventional uncertainty

We assume the uncertainties on angles to be known. Let start by the definition of variance applied to $\mathcal{S}$ and consider small displacement of $\mathcal{S}$:

$$\sigma^2_{\mathcal{S}(\boldsymbol{x},l)} = E\left[(\mathcal{S}(\boldsymbol{x},l) - E\left[\mathcal{S}\left(\boldsymbol{x},l\right)\right])^2\right] = E\left[(\mathrm{d}\mathcal{S}(\boldsymbol{x},l))^2\right]. \quad \text{(A.1)}$$

The differential of $\mathcal{S}$ includes partial derivatives with respect to the angle at position $\boldsymbol{x}$ and each angle at positions $\boldsymbol{x}+\boldsymbol{l_i}$, with $i \in [1, N]$:

$$\mathrm{d}\mathcal{S}(\boldsymbol{x},l) = \frac{\partial \mathcal{S}(\boldsymbol{x},\boldsymbol{l})}{\partial \psi(\boldsymbol{x})}\mathrm{d}\psi(\boldsymbol{x}) + \sum_{i=1}^{N}\left[\frac{\partial \mathcal{S}}{\partial \psi(\boldsymbol{x}+\boldsymbol{l_i})}\mathrm{d}\psi(\boldsymbol{x}+\boldsymbol{l_i})\right]. \quad \text{(A.2)}$$

When developing the square, one has:

$$\begin{aligned}(\mathrm{d}\mathcal{S}(\boldsymbol{x},l))^2 \;=\; & \left(\frac{\partial \mathcal{S}(\boldsymbol{x},l)}{\partial \psi(\boldsymbol{x})}\right)^2 (\mathrm{d}\psi(\boldsymbol{x}))^2 \\ & + \sum_{i=1}^{N}\left(\frac{\partial \mathcal{S}(\boldsymbol{x},l)}{\partial \psi(\boldsymbol{x}+\boldsymbol{l_i})}\right)^2 (\mathrm{d}\psi(\boldsymbol{x}+\boldsymbol{l_i}))^2 \\ & + 2\sum_{i=1}^{N}\frac{\partial \mathcal{S}(\boldsymbol{x},l)}{\partial \psi(\boldsymbol{x})}\frac{\partial \mathcal{S}(\boldsymbol{x},l)}{\partial \psi(\boldsymbol{x}+\boldsymbol{l_i})}\,\mathrm{d}\psi(\boldsymbol{x})\,\mathrm{d}\psi(\boldsymbol{x}+\boldsymbol{l_i}).\end{aligned} \quad \text{(A.3)}$$

If one takes the expectation of $\mathrm{d}\mathcal{S}^2$, then

$$\begin{aligned}E[\mathrm{d}\mathcal{S}(\boldsymbol{x},l)^2] \;=\; & \left(\frac{\partial \mathcal{S}(\boldsymbol{x},l)}{\partial \psi(\boldsymbol{x})}\right)^2 \sigma^2_{\psi(\boldsymbol{x})} + \sum_{i=1}^{N}\left(\frac{\partial \mathcal{S}(\boldsymbol{x},l)}{\partial \psi(\boldsymbol{x}+\boldsymbol{l_i})}\right)^2 \sigma^2_{\psi(\boldsymbol{x}+\boldsymbol{l_i})} \\ & + 2\sum_{i=1}^{N}\frac{\partial \mathcal{S}(\boldsymbol{x},l)}{\partial \psi(\boldsymbol{x})}\frac{\partial \mathcal{S}(\boldsymbol{x},l)}{\partial \psi(\boldsymbol{x}+\boldsymbol{l_i})}\,\sigma_{\psi(\boldsymbol{x})\psi(\boldsymbol{x}+\boldsymbol{l_i})}.\end{aligned} \quad \text{(A.4)}$$

The partial derivatives are:

$$\frac{\partial \mathcal{S}(\boldsymbol{x},l)}{\partial \psi(\boldsymbol{x})} = \frac{1}{2}\left(\frac{1}{N}\sum_{i=1}^{N}[\psi(\boldsymbol{x}) - \psi(\boldsymbol{x}+\boldsymbol{l_i})]^2\right)^{-1/2}\left(\frac{2}{N}\sum_{i=1}^{N}[\psi(\boldsymbol{x}) - \psi(\boldsymbol{x}+\boldsymbol{l_i}]\right),$$

$$\frac{\partial \mathcal{S}(\boldsymbol{x},l)}{\partial \psi(\boldsymbol{x}+\boldsymbol{l_i})} = -\frac{1}{2}\left(\frac{1}{N}\sum_{i=1}^{N}[\psi(\boldsymbol{x}) - \psi(\boldsymbol{x}+\boldsymbol{l_i})]^2\right)^{-1/2}\frac{2}{N}\left(\psi(\boldsymbol{x},\boldsymbol{l}) - \psi(\boldsymbol{x}+\boldsymbol{l_i})\right);$$

$$\begin{aligned}\left(\frac{\partial \mathcal{S}(\boldsymbol{x},l)}{\partial \psi(\boldsymbol{x})}\right)^2 &= \frac{1}{N^2}\left(\frac{1}{N}\sum_{i=1}^{N}[\psi(\boldsymbol{x}) - \psi(\boldsymbol{x}+\boldsymbol{l_i})]^2\right)^{-1} \\ &\quad \times \left(\sum_{i=1}^{N}[\psi(\boldsymbol{x}) - \psi(\boldsymbol{x}+\boldsymbol{l_i})]\right)^2 \\ &= \frac{\left(\sum_{i=1}^{N}[\psi(\boldsymbol{x}) - \psi(\boldsymbol{x}+\boldsymbol{l_i})]\right)^2}{N^2[\mathcal{S}(\boldsymbol{x},l)]^2}\end{aligned} \quad \text{(A.5)}$$

$$\left(\frac{\partial \mathcal{S}(\boldsymbol{x},l)}{\partial \psi(\boldsymbol{x}+\boldsymbol{l_i})}\right)^2 = \frac{[\psi(\boldsymbol{x}) - \psi(\boldsymbol{x}+\boldsymbol{l_i})]^2}{N^2[\mathcal{S}(\boldsymbol{x},l)]^2}. \quad \text{(A.6)}$$

As the noise levels on two measurements of polarization angle at different positions are uncorrelated, one has:

$$\sigma_{\psi(\boldsymbol{x})\psi(\boldsymbol{x}+\boldsymbol{l_i})} = 0.$$

Since $E[\mathrm{d}\mathcal{S}(\boldsymbol{x},l)^2] = \sigma^2_{\mathcal{S}(\boldsymbol{x},l)}$, Eq. (A.3) becomes

$$\begin{aligned}\sigma^2_{\mathcal{S}(\boldsymbol{x},l)} = \frac{1}{[N\mathcal{S}(\boldsymbol{x},l)]^2}\Bigg[&\left(\sum_{i=1}^{N}\left[\psi(\boldsymbol{x}) - \psi(\boldsymbol{x}+\boldsymbol{l_i})\right]\right)^2 \sigma^2_{\psi(\boldsymbol{x})} \\ &+ \sum_{i=1}^{N}(\psi(\boldsymbol{x}) - \psi(\boldsymbol{x}+\boldsymbol{l_i}))^2\sigma^2_{\psi(\boldsymbol{x}+\boldsymbol{l_i})}\Bigg].\end{aligned} \quad \text{(A.7)}$$

Taking the square root of this expression, one gets the conventional uncertainty on polarization angle dispersion function:

$$\begin{aligned}\sigma_{\mathcal{S},\mathrm{C}} = \frac{1}{N\mathcal{S}(\boldsymbol{x},l)}\Bigg[&\left(\sum_{i=1}^{N}\left[\psi(\boldsymbol{x}) - \psi(\boldsymbol{x}+\boldsymbol{l_i})\right]\right)^2 \sigma^2_{\psi(\boldsymbol{x})} \\ &+ \sum_{i=1}^{N}\left[\psi(\boldsymbol{x}) - \psi(\boldsymbol{x}+\boldsymbol{l_i})\right]^2\sigma^2_{\psi(\boldsymbol{x}+\boldsymbol{l_i})}\Bigg]^{1/2}.\end{aligned} \quad \text{(A.8)}$$